Global anisotropy and the thickness of continents

Yuancheng Gung , Barbara Romanowicz and Mark Panning

Berkeley Seismological Laboratory and Department of Earth and Planetary Science, Berkeley, CA, 94720,USA.

Since the concept of "tectosphere" was first proposed[1], there have been vigorous debates about the depth extent of continental roots[2,3]. The analysis of heat flow[4], mantle xenoliths[5], gravity and glacial rebound data[6] indicate that the coherent, conductive part of continental roots is not much thicker than 200−250 km. Some global seismic tomographic models agree with this estimate but others indicate much thicker lithosphere under old continents[7−11], reaching at least 400km in depth. Here we show that the disagreement can be reconciled when taking into account anisotropy. Significant radial anisotropy with Vsh>Vsv is present under most cratons in the depth range 250−400 km, similar to that reported earlier[12] at shallower depths (80−250km) under ocean basins. We propose that in both cases, this anisotropy is related to shear in the asthenospheric channel, located at different depths under continents and oceans. The seismically defined lithosphere is then at most 200−250 km thick under continents. The Lehmann discontinuity, observed mostly under continents around 200−240 km, and the Gutenberg discontinuity, observed under oceans at shallower depths (~ 60−80km), may both be associated with the bottom of the lithosphere, marking a transition to flow−induced asthenospheric anisotropy.

The maximum thickness of the lithosphere, defined as a region of distinctly faster than average seismic velocities (1.5−2%) in global S velocity tomographic models, ranges from 200−400 km, depending on the model[7−11]. This is manifested by a drop in correlation between some models from ~0.80 at 100km to less than 0.45 at 300 km

depth (Figure1a), which casts some doubt on the ability of global tomography to accurately resolve upper mantle structure. However, although global Vs models differ from each other significantly in the depth range 200−400km under the main continental shields, these differences are consistent when they are classified into three categories, depending on the type of data used to derive them: 'SV' (mostly vertical or longitudinal component data, dominated by Rayleigh waves in the upper mantle),'SH'(mostly transverse component data, dominated by Love waves), and 'hybrid' (3 component data). 'SH' and 'hybrid' models are better correlated with each other than with 'SV' models, and this difference is accentuated when the correlation is computed only across continental areas (Figure 1b). Also, 'SH' (and 'hybrid') models exhibit continental roots that exceed those of 'SV' models by 100 km or more, as illustrated in Figure 2 (see also supplementary material,Figure 1sup).

On the other hand, global tomographic studies that account for seismic anisotropy, either by inverting separately for Vsv and Vsh[12], or in the framework of more general anisotropic theory[13,14] , have documented significant lateral variations in the anisotropic parameter $\xi=(Vsh/Vsv)^2$ on the global scale. Until now, attention has mostly focused on the strong positive $\delta\ln\xi$ ($\delta\ln Vsh > \delta\ln Vsv$) observed in the central part of the Pacific Ocean in the depth range 80−200 km. The presence of this anisotropy has been related to shear flow in the asthenosphere, with a significant horizontal component. Deeper anisotropy was not well resolved in these studies, either because the dataset was limited to fundamental mode surface waves[13,], or because of the use of inaccurate depth sensitivity kernels[12]. In particular, it is important to verify that any differences in Vsv and Vsh observed below 200km depth are not an artifact of simplified theoretical assumptions, which ignore coupling by anisotropy[15]. Indeed, while coupling effects are relatively minor for fundamental mode surface waves they are non−negligible for higher modes (see Figure 2sup, in supplementary material).

We have developed an inversion procedure for transverse isotropy using three component surface and body waveform data, in the framework of normal mode asymptotic coupling theory[16], which in particular, involves the use of 2D broadband anisotropic sensitivity kernels appropriate for higher modes and body waves (see methods section). Figure 3 shows a comparison of the distributions of δlnVsh, δlnVsv and δlnξ in the resulting degree 16 anisotropic model (SAW16AN), at depths of 175 km, 300 km and 400 km. At 175 km depth, the global distribution of δlnξ confirms features found in previous studies, and is dominated by the striking positive (Vsh>Vsv) anomaly in the central Pacific[12] , and a similar one in the Indian Ocean. However, at depths greater than 250 km, the character of the distribution changes: positive δlnξ emerges under the Canadian Shield, Siberian Platform, Baltic Shield, southern Africa, Amazonian and Australian cratons, while the difference between Vsh and Vsv fades out under the Pacific and Indian oceans. At 300 km depth, the roots of most cratons are only visible in the Vsh maps, in which they extend down to about 400 km. Interestingly, the East Pacific Rise has a signature with δlnξ <0 down to 325km, indicative of a significant component of vertical flow. At 400 km depth, we also note that subduction zones in the western Pacific and south America are more prominent in the Vsv map, resulting in negative δlnξ around the Pacific ring. These features are emphasized in depth cross sections (Figure 4) across major continental shields, where we compare Vsh and Vsv distributions, consistently showing deeper continental roots in Vsh.

Temperatures in the 250−400 km depth range exceed 1000^{o}C, and are therefore too high to allow sustained frozen anisotropy in a mechanically coherent lithospheric lid on geologically relevant time scales[17]. Therefore we infer that the observed anisotropy mostly reflects shear in the asthenosphere, with a significant horizontal component, similarly to what is inferred in the Pacific Ocean at shallower depths. The difference in

depth range results simply from the difference in lithospheric thickness under continents and oceans. Thus lithospheric thickness under continents need not be larger than 200−250km, and seismic tomographic models can be reconciled with each other as well as with results from other geophysical studies.

Another issue greatly debated in the literature is the nature of the Lehmann discontinuity[18] (L), and in particular the puzzling observation that it is not a consistent global feature[19], and is observed mostly in continental areas[20] and not under oceans[21]. Leven et al.[22] first proposed that L might be an anisotropic discontinuity. Different models have been suggested, including transitions (with increasing depth) from anisotropic to isotropic, isotropic to anisotropic, or a boundary between two styles of anisotropy[23,24]. The global tomography results discussed here tend to favor one of the latter two models, with L representing the limit between an isotropic or weakly anisotropic lower lithosphere and an anisotropic asthenosphere under cratons. Under oceans, the lithosphere is much thinner, and the lithosphere/asthenosphere boundary occurs at much shallower depths. There is no consistently observed discontinuity around 200−250km km depth[20]. On the other hand, a shallower discontinuity, the Gutenberg discontinuity (G), is often reported under oceans and appears as a negative impedance reflector in studies of precursors to multiple ScS[21]. The difference in depth of the observed $\delta \ln \xi > 0$ anisotropy between continents and oceans is consistent with an interpretation of the L and G discontinuities as both marking the bottom of the mechanically coherent lithosphere.

In this study, we only consider transverse isotropy, which in particular does not account for intermediate orientation of the fast axis of anisotropy. We can only infer that regions with significant $\delta \ln \xi > 0$ are regions where anisotropy has a significant horizontal component, and expresses the alignment of olivine crystals in predominantly

horizontal flow. In ocean−continent transition regions, the asthenospheric flow would follow the inclined shape of the bottom of the lithosphere and be less clearly detected with our approach. In regions of subduction, there is no low viscosity asthenospheric channel. The horizontal flow under major continental roots is also consistent with recent results of attenuation tomography in the upper mantle[25], which indicate that upwelling from the transition zone above the African "superplume" spreads horizontally under the african lithosphere.

In conclusion, the inspection of radial anisotropy in the depth range 200−400 km allows us to infer that continental roots do not extend much beyond 250km depth, in agreement with other geophysical inferences. Tomographic models reveal the varying depth of the top of the anisotropic asthenospheric channel, marked by a detectable seismic discontinuity called L under continents, and G under oceans. Seemingly incompatible tomographic models obtained by different researchers can thus also be reconciled: the relatively poor correlation between different models in the depth range 250−400 km is not due to a lack of resolution of the tomographic approach, but rather to the different sensitivity to anisotropy of different types of data.

'Methods'.

A medium with radial anisotropy is described by 5 elastic parameters, A,C,F,L,N, and density ρ[26] . We start by considering, equivalently, the 6 parameters Vsh, Vsv, η=F/(A−2L), Vp_{iso} (isotropic Vp), ϕ=C/A and ρ, with appropriate kernels for weak transverse anisotropy. To reduce the number of parameters in the inversion and keep only those that are best resolved ($Vsh=(N/\rho)^{1/2}$, $Vsv= (L/\rho)^{1/2}$), we assume the following scaling relations, as inferred from laboratory experiments for depths relevant to our study (i.e. less than 500km)[27] :

$\delta \ln Vp_{iso} = 0.5\, \delta \ln Vs_{iso}$, $\delta \ln \eta = -2.5\, \delta \ln \xi$ and $\delta \ln \phi = -1.5\, \delta \ln \xi$, with

$\delta \ln Vs_{iso} = 2/3 \delta \ln Vsv + 1/3 \delta \ln Vsh$ (weak anisotropy) and $\delta \ln \rho = 0.3 \delta \ln Vs_{iso}$. We have verified that our results are not affected by the particular values chosen in these relations. Starting from our most recent tomographic models, SAW24B16[9] for Vsh and SAW16BV[25] for Vsv, we invert for perturbations in Vsh and Vsv in a spherical harmonics expansion up to degree 16 laterally. Vertical parametrization is in terms of cubic splines. Since our sampling of the lowermost mantle with SV−sensitive body waves is limited, in order to avoid bias from anisotropy in D'', we have restricted our inversion to the top 1500km of the mantle, and chosen the body waveforms to include in the dataset accordingly.

We have checked that our results, and in particular the observation of radial anisotropy under continents at depths greater than 200 km is not the result of artifacts due to poor resolution in the inversion for either Vsh or Vsv, by performing synthetic tests. For example, Figure 3sup (supplementary Information) shows the results of an experiment in which synthetic transverse component seismograms have been computed for a starting SV model (no roots below 250 km), mimicking the actual distribution of our dataset, and then reinverted for an SH model. No deep continental roots are apparent in the resulting final model.

1. Jordan. T. H., The continental lithosphere, *Rev. Geoph. Space Phys.*, **13**, 1−12 (1975).

2. Anderson, D. L., The deep structure of continents, J. Geophys. Res., 84, 7555−7560 (1990).

3. Artemieva, I. M. And Mooney, W., Thermal thickness and evolution of Precambrian lithosphere: a global study, J. Geophys. Res., 106, 16,387−16,414 (2001).

4. Jaupart, C., Mareschal, J. C. & Guillou−Frottier, L., Heat flow and thickness of the lithosphere in the Canadian Shield, *J. Geophys. Res*., **103**, 15,269−15,286 (1998).

5. Rudnick, R., McDonough, W. & and O'Connell, R. Thermal structure, thickness and composition of continental lithosphere, *Chem. Geol*., **145**, 395−411 (1998)

6. Peltier, W. R., The thickness of the continental lithosphere, *J. Geophys. Res.*, **89**, 11,303−11,316 (1984).

7. Ritsema, J. , van Heijst H. & Woodhouse , J. H. , Complex shear wave velocity structure imaged beneath Africa and Iceland, *Science*, **286**, 1925−1928, (1999).

8. Grand S. P., van der Hilst R. & Widiyantoro S. Global seismic tomography: a snapshot of convection in the Earth, *GSA Today*, **7**, 4, 1−7 (1997).

9. Mégnin C & Romanowicz B. The 3D shear velocity structure of the mantle from the inversion of body, surface and higher mode waveforms, *Geophys. J. Int*., **143**, 709−728 (2000).

10.Gu, Y. J., A.. M. Dziewonski, Su, W.−J. & G. Ekström, G., Models of the mantle shear velocity and discontinuities in the pattern of lateral heterogeneities, *J. Geophys. Res.*, **106**, 11169−11199 (2001).

11.Masters G., Johnson, S., Laske, G. and Bolton, B., 1996. A shear−velocity model of the mantle, *Philos. Trans. R. Soc. Lond. A*, **354**, 1,385−1,411.

12.Ekström, G. &. Dziewonski, A. M. The unique anisotropy of the Pacific upper mantle, *Nature*, **394**, 168−172 (1998).

13.Montagner J. P. & Tanimoto T. Global upper mantle tomography of seismic velocities and anisotropy, *J. Geophys. Res.*, **96**, 20,337−20,351 (1991).

14.Babuska V, Montagner J. P., Plomerova J. & Girardin N. Age−dependent large−scale fabric of the mantle lithosphere as derived from surface wave velocity anisotropy, *Pure Appl. Geophys.*, **121**, 257−280 (1998).

15.Regan, J. & Anderson, D. L. Anisotropic models of the upper mantle, *Phys. Earth Planet. Inter.*, **35**, 227−263 (1984).

16.Li, X. D. & Romanowicz B. Comparison of global waveform inversions with and without considering cross branch coupling, *Geophys. J. Int*., **121**, 695−709 (1995).

17.Vinnik, L. P. , Makeyeva, L. I., Milev A. & and Usenko A. Yu., Global patterns of azimuthal anisotropy and deformations in the continental mantle, *Geophys. J. Int*., **111**, 433−447 (1992).

18.Bina, C. R., Mantle discontinuities, *Rev. of Geophys. Suppl*., 783−793 (1991).

19.Shearer, P., Seismic imaging of upper mantle structure with new evidence for a 520km discontinuity, *Nature*, **344**, 121−126 (1990).

20.Gu, Y M., Dziewonski, A. M. & Ekstr\"om, G. Preferential detection of the Lehmann discontinuity beneath continents, *Geophys. Res. Lett*., **28**, 4655−4658 (2001).

21.Revenaugh, J. & Jordan, T. H ., Mantle layering from ScS reverberations, 3. The upper mantle, *J. Geophys. Res*., **96**, 19781−19810 (1991).

22.Leven, J. H., Jackson, I. & Ringwood, A. E.Upper mantle seismic anisotropy and lithospheric decoupling, *Nature*, **289**, 234− (1981).

23.Karato, S. I. On the Lehmann discontinuity, *Geophys. Res. Lett*., **19**, 2255−2258 (1992).

24. Gaherty, J. B. & Jordan, T. H. Lehmann discontinuity as the base of an anisotropic layer beneath continents, *Science*, **268**, 1468−1471 (1995).

25. Romanowicz,B. and Gung, Y. C., Superplumes from the core−mantle boundary to the lithosphere: implications for heat flux, *Science*, **296**, 513−516 (2002).

26. Love, A. E. H., *A Treatise on the theory of elasticity*, 4th edn (Cambridge Univ., (1927).

27. Montagner, J. P. and Anderson, D. L., Petrological constraints on seismic anosotropy, *Phys. Earth Planet. Int*, **54**, 82−105 (1989).

28. Mooney, W. D., Laske, G. & Masters, G. , CRUST−5.1: A global crustal model at 5° x 5°, *J. Geophys. Res.*, **103**, 727−747 (1998).

29. Dziewonski A. M. & Anderson D.L., Preliminary Reference Earth Model. *Phys. Earth Planet. Int.*, **25**, 297−356 (1981).

'**Supplementary Information** accompanies the paper on *Nature*'s website (http://www.nature.com).

<ack> Style tag for the Acknowledgements and the Competing Interests statement.

Correspondence and requests for materials should be addressed to Y.G. (e−mail: gung@seismo.berkeley.edu).

Figure 1. Correlation coefficient as a function of depth between model SAW24B16[9], an 'SH' model, and other global tomographic S velocity models. a)

correlation computed over the whole globe; b) correlation computed over continental areas only. Here continents include all areas of elevation greater than −0.5 km and is based on model Crust5.1[28]. Note that models S20A_SH[12] (an "SH" model) and S362D1[10] (a "hybrid model") correlate better with SAW24B16 than models S20A_SV[12] and S20RTS[7], which are both "SV" models. The reduced correlation in the depth range 250−400 km between "SH/hybrid" models and "SV" models is strongly accentuated over continents.

Figure 2. Maximum depth for which the velocity anomaly with respect to the reference model PREM[29] is greater than 2%, for different S velocity models. Left: "SH" type models; right: "SV" type models. Bottom: Vsh model SAW24B16[9] compared to Vsv model S20RTS[7]; middle: SH and SV parts of model S20A[12], obtained by inverting T component data and Z,L component data separately; top: SH and SV parts of anisotropic model SAW16SH discussed here. While the roots of continents generally extend to depths greater than 300−350 km in SH models, they do not exceed 200−250km in SV models.

Figure 3. Maps of relative lateral variations in anisotropic model SAW16AN at 3 depths in the upper mantle. Left: $\delta \ln Vsh$; middle: $\delta \ln Vsv$; right: $\delta \ln \xi = 2(\delta \ln Vsh - \delta \ln Vsv)$. $\delta \ln \xi > 0$ in regions where Vsh>Vsv and $\delta \ln \xi < 0$ in regions where Vsv<Vsh. Lateral variations are referred to reference model PREM[29], which is isotropic below 220km depth. Note how the regions of strong positive $\delta \ln \xi$ shift from the central Pacific to continental areas between 175 and 300 km depth. At depths shallower than 200km, continental shields have mostly $\delta \ln \xi < 0$, as noted previously[14]. At 300 km depth, continental shields are no longer prominent in Vsv. At depths greater than 350km, the subduction zones are more prominent in Vsv than in Vsh,resulting in $\delta \ln \xi < 0$ around the Pacific, indicative of vertical

flow. The East Pacific rise appears as a zone of vertical flow to depths in excess of 300km.

Figure 4. Depths cross−sections through 3 continents (see location at top) showing the SH (left) and SV(right) components of anisotropic model SAW16AN. The SH sections consistently indicate fast velocities extending to depths in excess of 220 km, whereas the SV sections do not. In section B, the higher velocity associated with the subduction under Kamtchatka is clearly visible in SV but not so much in SH. This anisotropy may explain why subduction zones are generally less visible in S tomographic models (mostly of the "hybrid" type) than in P models.

Supplementary material

Figure 1sup. Depth cross−sections across the Canadian Shield, for different SH/hybrid (left) and SV (right) global tomographic models.From bottom to top: left) hybrid models SB4L18[11], S362D1[10] and SH model SAW24B16[8]; right) SV models S20RTS[7], S20A_SV[12] and SAW16BV[25].The models on the left consistently exhibit continental roots that exceed 220 km depth, whereas the models on the right do not.

Figure 2sup. Examples of depth sensitivity kernels for toroidal modes ${}_0T_{40}$ (left) and ${}_1T_{40}$ (right), comparing the case of an isotropic Vs model (grey line), with that of an anisotropic Vs model (PREM[29], black continuous and dotted lines). For the fundamental mode, there is not much difference between isotropic and anisotropic Vsh, whereas for the overtone, the difference is significant in the first 400 km in depth.

Figure 3sup. Results of synthetic test in which an input model (middle panels) of the "SV" type is considered (without deep lithospheric roots). Synthetic

seismograms for SH component data with the same distribution as our real data collection are computed. The synthetic data thus obtained are then inverted for SH structure, starting from an SH model (SAW24B16) which exhibits deep continental roots (left panels). In the resulting inverted model,no deep continental roots have appeared, consistent with the input model. The rightmost panel shows the correlation as a function of depth of the output model, with, respectively, the input model (SV) and the starting model (SH). The results of this test indicate that the differences in SH and SV models in the depth range 250−400km are not due to an artifact in the inversion process, and in particular to the different depth sensitivity of various SH and SV sensitive phases present in the data.

Figure 1

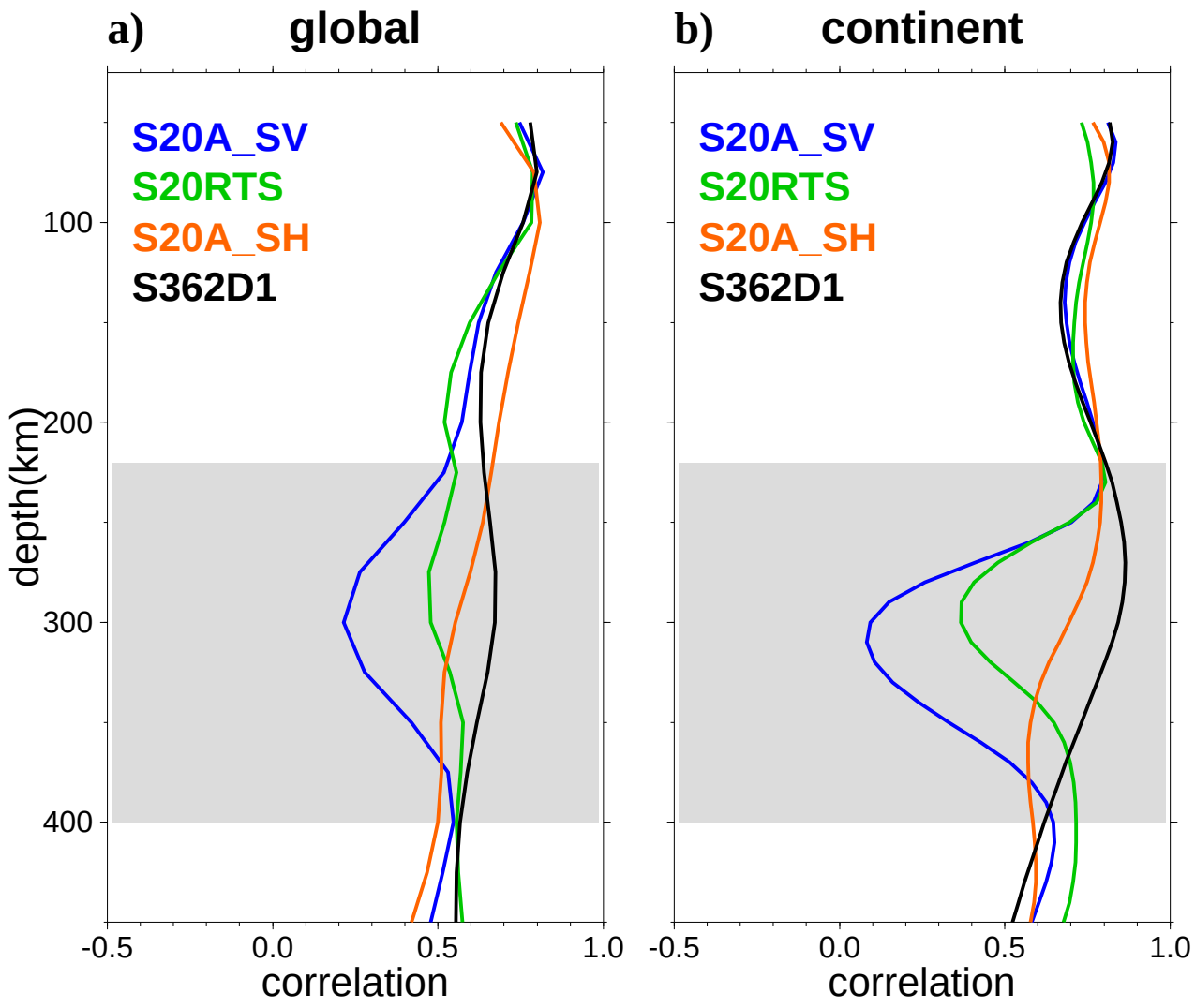
a)
global
b)
continent
S20A_SV
S20RTS
S20A_SH
S362D1
depth(km)
100
200
300
400
-0.5
0.0
0.5
1.0
correlation

Figure 2

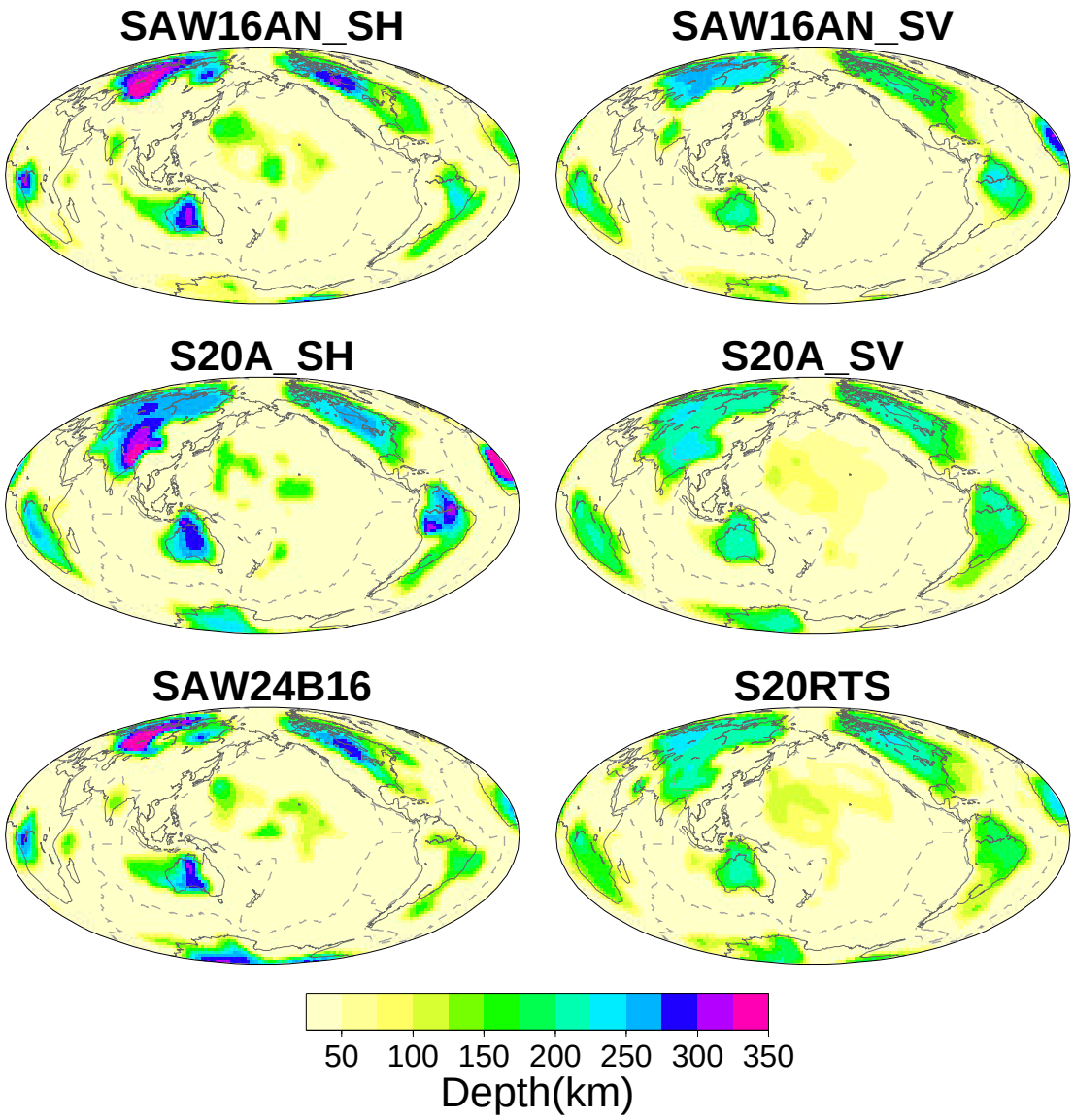
SAW16AN_SH
SAW16AN_SV
S20A_SH
S20A_SV
SAW24B16
S20RTS
50
100
150
200
250
300
350
Depth(km)

Figure 3

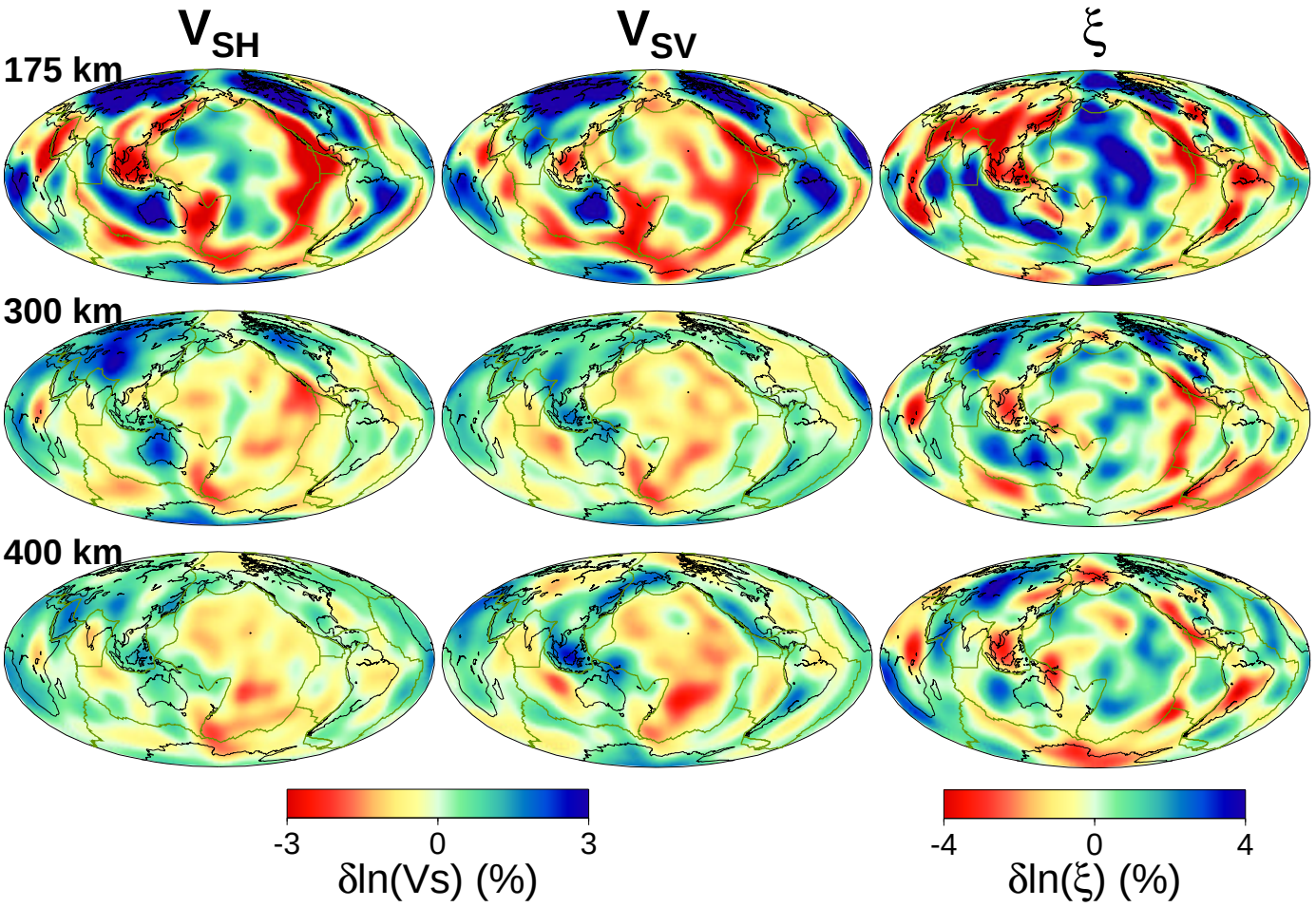

Figure 4

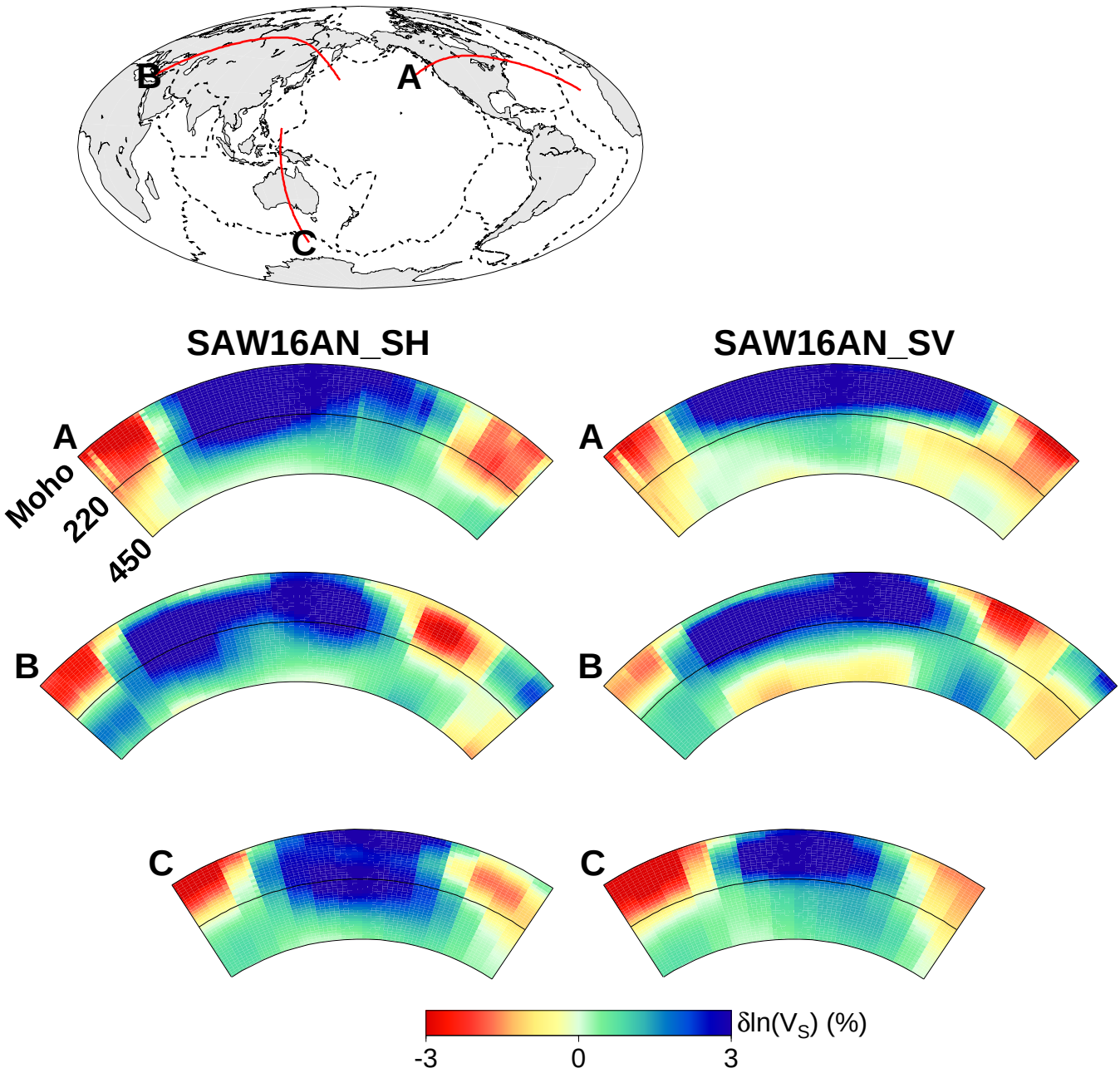

Figure1_sup

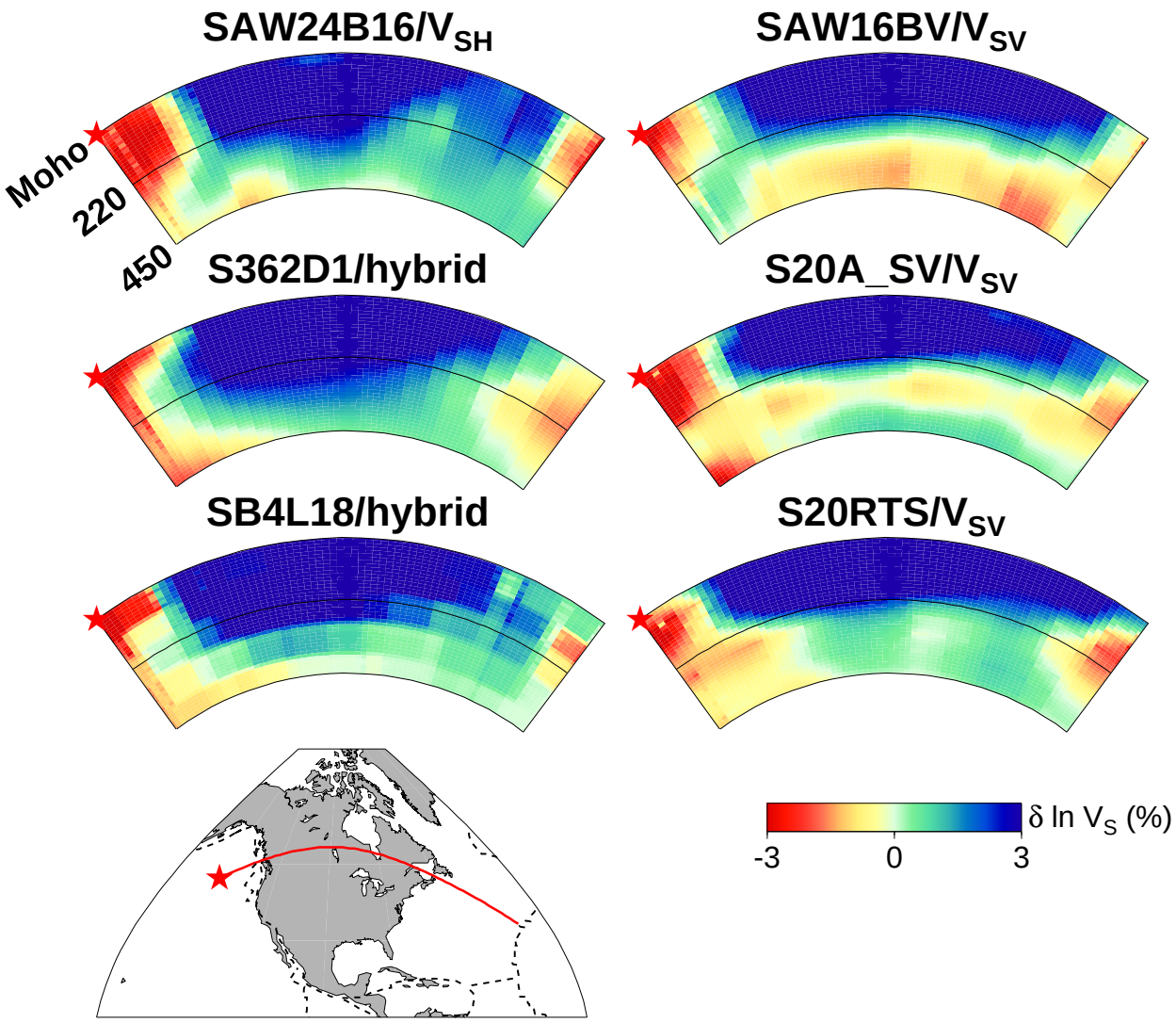
SAW24B16/V$_{SH}$
SAW16BV/V$_{SV}$
Moho
220
450
S362D1/hybrid
S20A_SV/V$_{SV}$
SB4L18/hybrid
S20RTS/V$_{SV}$
δ ln V$_S$ (%)
-3
0
3

Figure2_sup

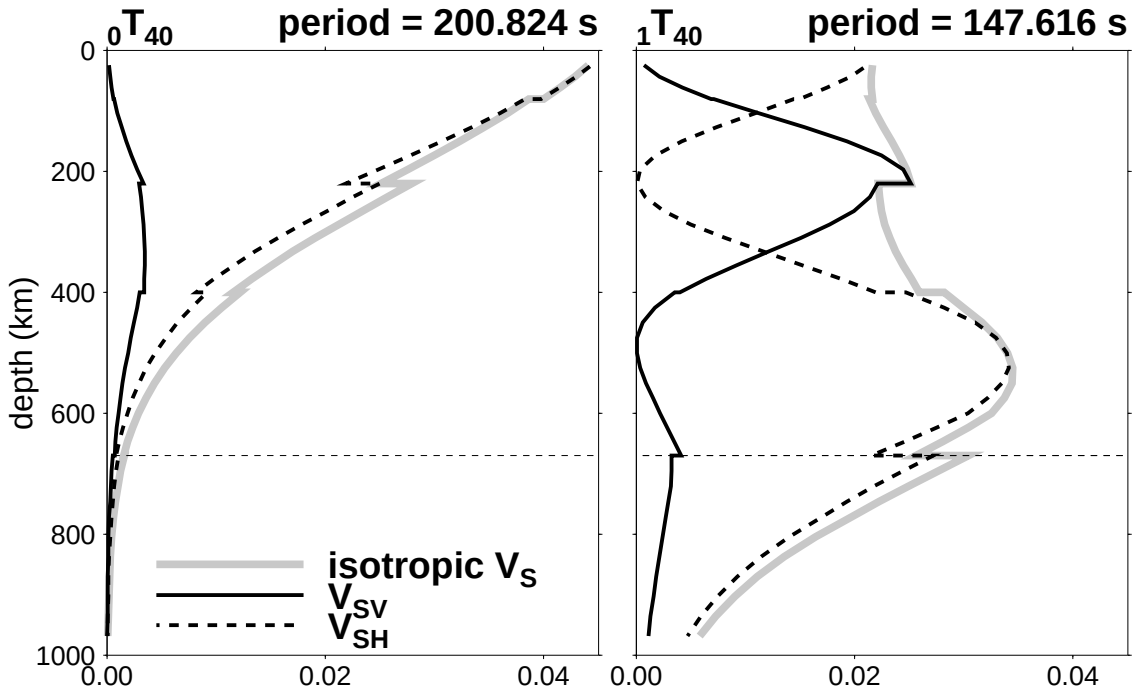
$_0T_{40}$
period = 200.824 s
$_1T_{40}$
period = 147.616 s
depth (km)
0
200
400
600
800
1000
0.00
0.02
0.04
isotropic V_S
V_{SV}
V_{SH}

Figure3_sup

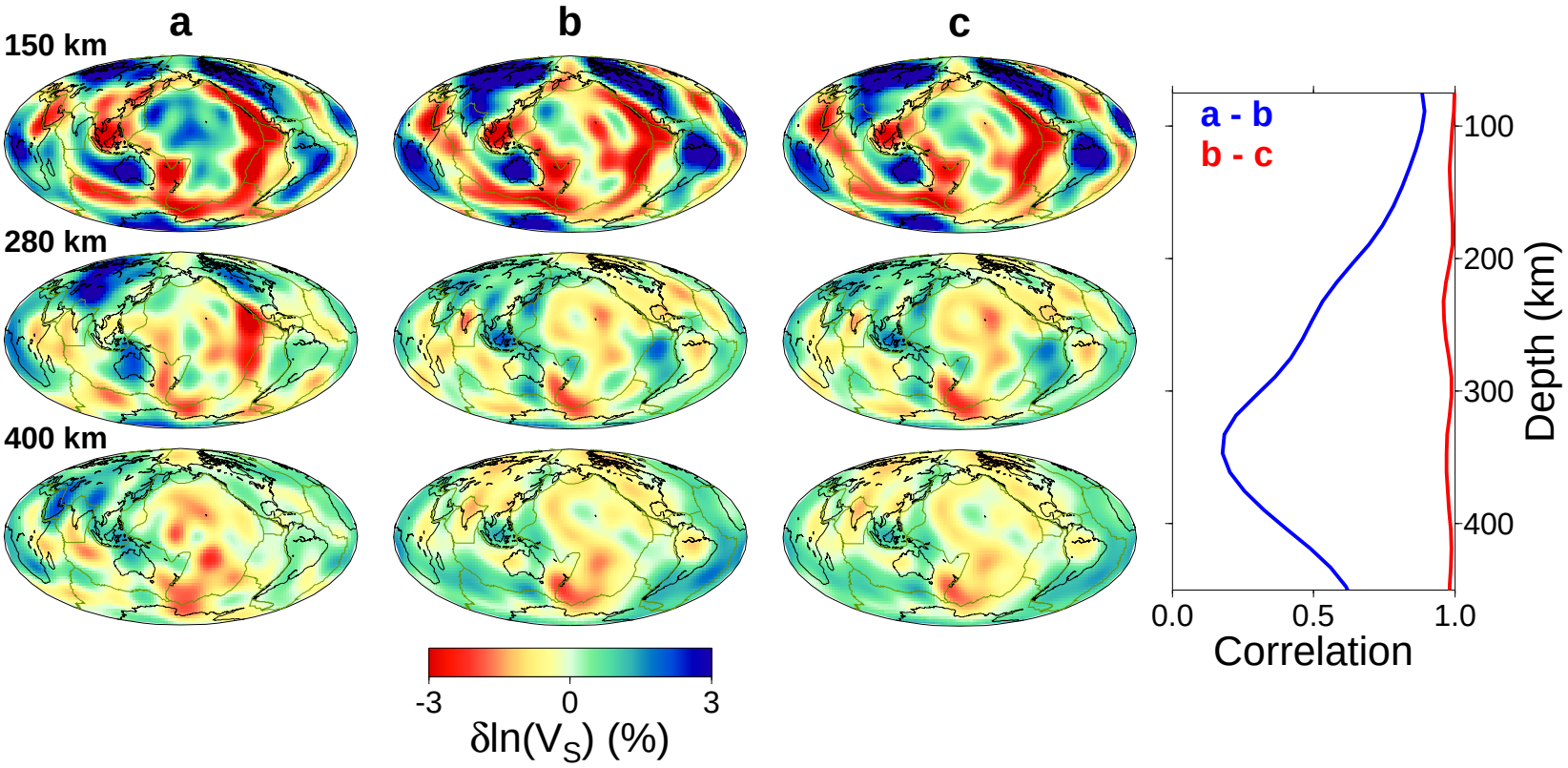
a
b
c
150 km
280 km
400 km
-3
0
3
δln(VS) (%)
a - b
b - c
100
200
300
400
Depth (km)
0.0
0.5
1.0
Correlation